Chandra Spectroscopy of the 70 Oph and 36 Oph Binaries

Brian E. Wood[1] and Jeffrey L. Linsky[1]

[1] JILA, University of Colorado, Boulder, CO 80309-0440, USA

Abstract

In the summer of 2004, *Chandra* observed 70 Oph (K0 V+K5 V) and 36 Oph (K1 V+K1 V), resolving these nearby binaries for the first time in X-rays. The LETG/HRC-S spectra of all four of these stars are presented and compared with a higher S/N archival LETG spectrum of another K dwarf, ϵ Eri (K1 V). All 5 moderately active K dwarfs turn out to have nearly identical coronal temperature distributions (e.g., emission measure distributions), but there are significant differences in their coronal abundances. The coronae and winds of the Sun and many solar-like stars have a curious abundance pattern where the abundances of elements with low first ionization potential (FIP) are enhanced relative to high FIP elements. Our 5 stars exhibit different degrees of FIP bias, with the two 70 Oph stars surprisingly representing opposite ends of the observed range. Any explanation for the FIP effect will have to explain how two stars so similar in all other respects (age, rotation rate, X-ray luminosity, spectral type) can have coronae with different degrees of FIP bias.

1. Observations

We report here on X-ray spectra obtained by *Chandra*'s Low Energy Transmission Grating (LETG), using the HRC-S detector. Our new observations from the summer of 2004 are of two moderately active K dwarf binaries, 70 Oph (K0 V+K5 V) and 36 Oph (K1 V+K1 V). *Chandra*'s superb spatial resolution allows these binaries, both with 5″ separations, to be resolved for the first time in X-rays. In addition to these data, we also analyze archival LETG/HRC-S spectra of another moderately active K dwarf, ϵ Eri (K1 V). Our goal is to compare the X-ray spectra of these 5 K dwarfs with very similar levels of coronal activity, in order to see if these stars have identical coronal properties.

The zeroth-order images of 36 Oph and 70 Oph provided by the LETG observations are shown in Figure 1, and Figure 2 shows light curves for these 4 stars plus ϵ Eri, which are obtained from the zeroth-order data. Some modest, gradual variability with a timescale of hours is present for our targets, but the closest thing to a flare is the peak seen for 36 Oph B at $t = 31$ ksec, where the flux briefly increases by about a factor of 2. The CIAO-processed LETG spectra are shown in Figure 3, where we have rebinned the data by a factor of 3 to improve S/N. The emission lines identified in the figure are measured, or upper limits are computed for nondetections, and these measurements provide the basis for the analysis that follows.

2. Flux Ratios and the FIP Effect

In the solar corona and solar wind, elemental abundances are generally found to be dependent on first ionization potential (FIP). Relative to reference solar photospheric abundances, elements with low FIP (Fe, Mg, Si, etc.) are generally found to have coronal abundances that are enhanced relative to elements with high FIP (C, N, O, Ne, etc.) (Feldman & Laming 2000). Evidence for this effect has been found for some stars of low to moderate activity (Laming et al. 1996; Drake et al. 1997; Laming & Drake 1999). However, on active stars the FIP effect is generally either absent or sometimes an inverse FIP effect is observed, where high FIP elements have coronal abundances that are *higher* relative to photospheric values than is the case for low FIP elements (Audard et al. 2003; Huenemoerder et al. 2003; Sanz-Forcada et al. 2003).

It is possible to see whether our sample of stars exhibits different levels of FIP bias simply by comparing line fluxes. The most dramatic difference is seen when comparing 70 Oph A and 70 Oph B, which is remarkable since these stars are members of the same binary! Figure 4 shows 70 Oph A/70 Oph B line flux ratios as a function of line formation temperature. The ratios for the low FIP elements (in green) are higher than those of the high FIP elements (in red) by about a factor of 3, indicating that 70 Oph A has a FIP effect that is stronger than its companion by about a factor of 3. There is no obvious temperature dependence for this effect.

Considering that 70 Oph A and B have the same age; and very similar rotation periods (19.7 and 22.9 days), coronal X-ray luminosities (see Fig 1), and spectral types (K0 V and K5 V), this difference is very hard to explain. What is the difference in the two stars that leads to different coronal abundances? The level of FIP bias for active regions on the Sun seems to depend on the age of the active region, with the FIP effect becoming more prominent the older the region (Feldman & Laming 2000). Perhaps at the time of observation, the visible part of 70 Oph B's corona was dominated by young active regions while the visible part of 70 Oph A's corona was dominated by old active regions, in which case the observed difference in FIP behavior is temporary.

Figure 5 shows a line ratio plot similar to Figure 4, but comparing 70 Oph A with ϵ Eri. In this case UV line fluxes from HST spectra, sampling lower temperature plasma, are also considered in addition to the *Chandra* measurements (Ayres et al. 2003; Sim & Jordan 2005). In the corona ($\log T > 5.8$), 70 Oph A has a stronger FIP effect than ϵ Eri (i.e., the line ratios of the low FIP lines are higher than the high FIP lines), but this is not clearly apparent in the transition region ($4.3 < \log T < 5.8$). It is widely assumed that the origin of the FIP effect must lie in the chromosphere ($3.8 < \log T < 4.3$), where the low FIP ions are ionized but the high FIP ions are not. So why does Figure 5 suggest different degrees of FIP bias in the transition region and corona? Perhaps the transition region emission arises in large part in different magnetic structures than the coronal emission, a conclusion supported by images of the Sun's corona and transition region, which have very different appearances (Feldman & Laming 1994).

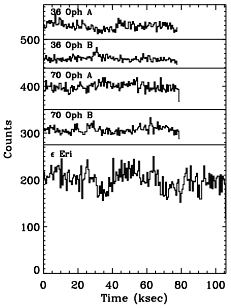

Figure 2: X-ray light curves for our targets computed from the zeroth-order images in the *Chandra* LETG/HRC-S data, using 10 minute time bins. Some modest, gradual variability with a timescale of hours is present, but the closest thing to a flare is the peak seen for 36 Oph B at $t = 31$ ksec.

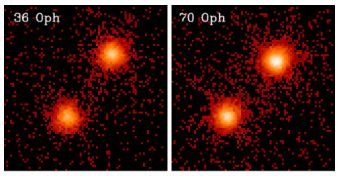

Figure 1: Zeroth-order images of 36 Oph and 70 Oph from *Chandra* LETG/HRC-S observations. North is up in the figures and in each case the A component is the upper right constituent of the binary. The stellar separation is about 5″ for both binaries.

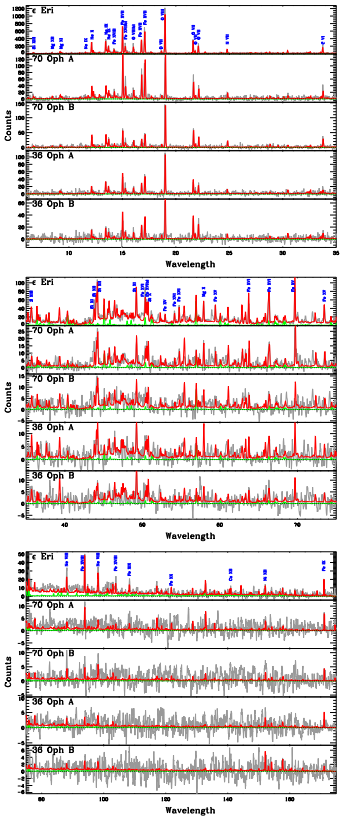

Figure 3: The *Chandra* LETG/HRC-S spectra of the 5 moderately active K dwarfs in our sample, rebinned by a factor of 3 to improve S/N. For wavelengths above 35 Å, the spectra are also smoothed for the sake of appearance. The red lines are synthetic spectra computed using the derived emission measure distributions and abundances shown in Figs. 6 and 8, and the green lines indicate the contributions of higher spectral orders (2–5) to the model spectra.

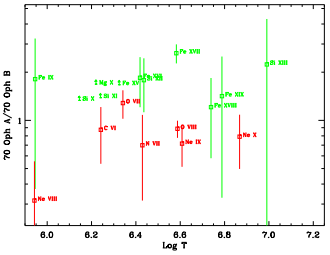

Figure 4: 70 Oph A/70 Oph B flux ratios for emission lines detected for both stars, plotted versus line formation temperature. In cases where there is more than one line for a given species, we simply add fluxes together for all lines detected for both stars. Higher ratios are clearly observed for lines of low FIP elements (green data points) than for high FIP elements (red data points). This indicates that the corona of 70 Oph A has a stronger FIP effect than 70 Oph B, a surprising result considering how similar these stars are (see text).

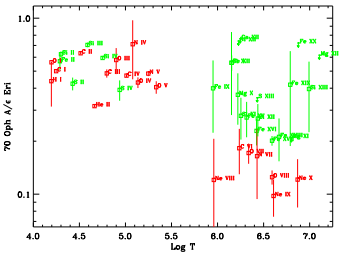

Figure 5: 70 Oph A/ϵ Eri flux ratios for *Chandra* X-ray and HST UV emission lines detected for both stars, plotted versus line formation temperature. High FIP and low FIP elements are in red and green, respectively. Analogous to the situation in Fig. 4, 70 Oph A clearly shows a stronger coronal FIP effect than ϵ Eri for $\log T > 5.8$, but this effect is not seen in the transition region ($4.3 < \log T < 5.8$) or chromosphere ($\log T < 4.3$).

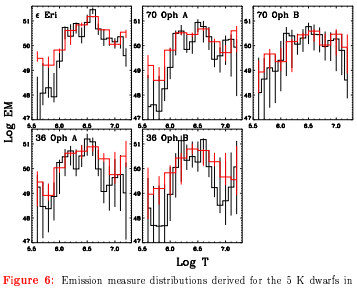

Figure 6: Emission measure distributions derived for the 5 K dwarfs in our sample, where we have experimented with two different temperature resolutions: a binning with $\Delta \log T = 0.1$ (black) and one with $\Delta \log T = 0.2$ (red). Error bars are 90% confidence intervals.

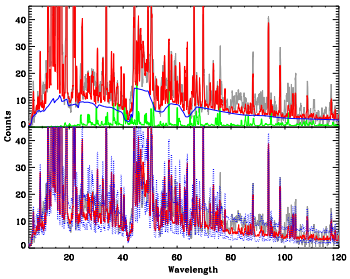

Figure 7: An illustration of how the line-to-continuum ratio is used to derive the absolute coronal Fe abundance, using ϵ Eri as an example. The bottom panel compares the highly smoothed stellar spectrum with a synthetic spectrum (red line) computed from the emission measure distribution in Fig. 6, assuming a best-fit absolute Fe abundance of $[\mathrm{Fe/H}] = 1.4[\mathrm{Fe/H}]_\odot$. Dotted blue lines show the effect of raising or lowering this value by a factor of 2, where the higher line corresponds to lower [Fe/H]. The upper panel shows the same fit, and also shows explicitly the continuum (blue line) and higher order (green line) contributions to the total line-plus-continuum model spectrum (red line).

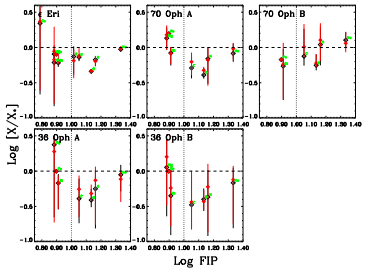

Figure 8: Coronal abundances relative to stellar photospheric abundances, where the error bars are 90% confidence intervals. The abundances are plotted versus first ionization potential (FIP) in eV. The dotted line crudely separates low-FIP and high-FIP elements. Black data points correspond with the black emission measure distributions in Fig. 6, and red data points correspond with the red distributions (with the coarser temperature binning). Error bars are meant to indicate the uncertainties in the abundances *relative to Fe*, so that is why the Fe uncertainties are zero.

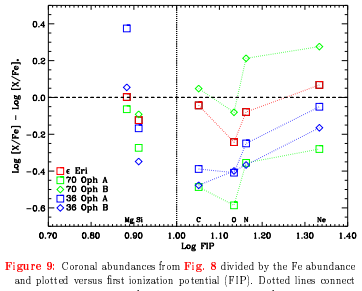

Figure 9: Coronal abundances from Fig. 8 divided by the Fe abundance and plotted versus first ionization potential (FIP). Dotted lines connect the high FIP abundances for each star, suggesting the following sequence of increasing FIP effect: 70 Oph B, ϵ Eri, 36 Oph A, 36 Oph B, 70 Oph A.

3. Emission Measure and Abundance Analysis

In order to quantify the coronal abundances and temperature distributions, we perform an emission measure (EM) analysis using the PINTofALE software developed by Kashyap & Drake (2000). Figure 6 shows EM distributions for the 5 stars in our sample, where we have experimented with two different temperature binnings. Our 5 moderately active K dwarfs show very similar EM distributions, all of which rise steeply from $\log T = 5.8$ to $\log T = 6.1$, all of which show a peak near $\log T = 6.6$, and all of which decline for $\log T > 6.7$.

The initial EM analysis is based solely on line measurements. Coronal abundances are measured relative to Fe, which is itself initially fixed to the solar photospheric abundance. In order to determine the absolute Fe abundance relative to H and properly normalize the EM distribution, it is necessary to assess the line-to-continuum ratio. Figure 7 illustrates this process for the case of ϵ Eri. The bottom panel shows a synthetic spectrum generated from the emission measure distribution in Figure 6, assuming an absolute Fe abundance of $[\mathrm{Fe/H}] = 1.4[\mathrm{Fe/H}]_\odot$, which is judged to lead to the best fit. In addition to the dominant first-order spectrum, we also take into account orders 2–5 in generating synthetic spectra. The lower panel shows what happens when [Fe/H] is raised or lowered by a factor of 2. The upper panel shows the same fit, and also shows explicitly the continuum (in blue) and higher order (in green) contributions to the total line-plus-continuum spectrum (in red). Our best-fit model spectra are compared with the data in Figure 3 for all of our stars.

Figure 8 illustrates the coronal abundances derived from this analysis, plotted versus FIP. Abundances are shown divided by stellar photospheric abundances from Allende Prieto et al. (2004) in order to correct for intrinsic stellar abundance variations. One unexpected result is that even in cases where a FIP effect appears to be present (70 Oph A, 36 Oph AB), the effect seems to be more of a case of high FIP elements being depleted in the corona rather than the low FIP elements being enhanced, which is the usual picture. Telleschi et al. (2005) find a similar effect in their sample of solar-like stars, and some analyses of solar X-ray spectra have also yielded this result (Fludra & Schmelz 1995). Does this imply that our entire empirical picture of the FIP effect needs revision, or are these results artifacts of missing X-ray lines that lead to overestimation of the true X-ray continuum level (see Fig. 7)?

For ease of comparison, Figure 9 plots the Mg, Si, C, O, N, and Ne abundances of all 5 stars from Figure 8 relative to Fe, as a function of FIP. The high FIP data points are connected with dotted lines, which suggests the following sequence of decreasing FIP bias: 70 Oph A, 36 Oph B, 36 Oph A, ϵ Eri, 70 Oph B. The remarkable difference between 70 Oph A and 70 Oph B has already been discussed in section 2. It is interesting that the relative abundances of the high-FIP elements are similar for all 5 stars, with Ne being particularly high and O being particularly low. Is this due to a real coronal abundance effect that favors Ne over O, or is this an artifact of uncertainties in the reference photospheric abundances? The issue of solar/stellar O and Ne abundances has become very muddy in the last few years (Allende Prieto et al. 2001; Bahcall et al. 2005; Drake & Testa 2005), too muddy to get into in any detail here! But it is worth noting that the Ne/O ratios seen for our 5 stars agree well with the Ne/O=0.41 average found from the large stellar sample of Drake & Testa (2005), which seems to be at least a factor of 2 larger than the solar coronal value (e.g., Acton et al. 1975; Young 2005). Does this difference indicate that either the solar or stellar measurements are wrong, or are the stellar Ne/O truly larger than the solar value (presumably due to the stars being of generally higher activity than the Sun)?

REFERENCES

Acton, L. W., Catura, R. C., & Joki, E. G. 1975, ApJ, 195, L93
Allende Prieto, C., Barklem, P. S., Lambert, D. L., & Cunha, K. 2004, A&A, 420, 183
Allende Prieto, C., Lambert, D. L., & Asplund, M. 2001, ApJ, 556, L63
Audard, M., Güdel, M., Sres, A., Raassen, A. J. J., & Mewe, R. 2003, A&A, 398, 1137
Ayres, T. R., Brown, A., Harper, G. M., Osten, R. A., Linsky, J. L., Wood, B. E., & Redfield, S. 2003, ApJ, 593, 993
Bahcall, J. N., Basu, S., & Serenelli, A. M. 2005, ApJ, 631, 1281
Drake, J. J., Laming, J. M., & Widing, K. G. 1997, ApJ, 478, 403
Drake, J. J., & Testa, P. 2005, Nature, 436, 525
Feldman, U., & Laming, J. M. 1994, ApJ, 436, 370
Feldman, U., & Laming, J. M. 2000, Phys. Scr., 61, 222
Fludra, A., & Schmelz, J. T. 1995, ApJ, 447, 936
Huenemoerder, D. P., Canizares, C. R., Drake, J. J., & Sanz-Forcada, J. 2003, ApJ, 595, 1131
Kashyap, V., & Drake, J. J. 2000, Bul. Astron. Soc. India, 28, 475
Laming, J. M., & Drake, J. J. 1999, ApJ, 516, 324
Laming, J. M., Drake, J. J., & Widing, K. G. 1996, ApJ, 462, 948
Sanz-Forcada, J., Maggio, A., & Micela, G. 2003, A&A, 408, 1087
Sim, S. A., & Jordan, C. 2005, MNRAS, 361, 1102
Telleschi, A., Güdel, M., Briggs, K., Audard, M., Ness, J.-U., & Skinner, S. L. 2005, ApJ, 622, 653
Young, P. R. 2005, A&A, submitted